Penerbit Akademia Baru

Journal of Advanced Research in Fluid Mechanics and Thermal Sciences

Journal homepage: www.akademiabaru.com/arfmts.html
ISSN: 2289-7879

Modelling Three Dimensional Unsteady Turbulent HVAC Induced Flow

Ahmed H Hafez[1,*], Tamer Heshmat Mohamed Aly Kasem[2], Basman Elhadidi[3], Mohamed Madbouly Abdelrahman[1]

[1] Aerospace Engineering Department, Cairo University, Egypt
[2] Smart Engineering Systems Research Centre (SESC), Nile University, Egypt
[3] School of Mechanical and Aerospace Engineering, Nanyang Technological University, Singapore

ARTICLE INFO

Article history:
Received 10 May 2021
Received in revised form 10 August 2021
Accepted 15 August 2021
Available online 6 September 2021

Keywords:
HVAC; Three-Dimensional Flow; Turbulence; Buoyancy Driven Flow

ABSTRACT

The number of words should not exceed 350. A three-dimensional numerical model for HVAC induced flow is presented. The nonlinear set of buoyancy driven incompressible flow equations, augmented with those of energy and k-ϵ turbulence model is solved. Various relevant are discussed. These challenges include avoiding expensive commercial packages, modelling complex boundaries, and capturing near wall gradients. Adaptive time stepping is employed to optimize computational effort. Three-dimensional simulation requirements are addressed using parallel computations. Two-dimensional and three-dimensional results are presented to clarify the model significance. Validation is done using full scale measurements. Good agreement with velocity and temperature profiles are illustrated.

1. Introduction

Residential and commercial buildings account for between 20% and 40% of total energy consumption, in developed countries [1]. Electricity worldwide is normally generated using fossil fuels [2]. Hence, effectively optimized HVAC operations mean billions of reduced tons of greenhouse emissions [3]. Consequently, accurate modeling of heating, ventilation, and air conditioning (HVAC) applications is crucial to avoid adverse effects on the earth's ecosystem [4].

Computational fluid dynamics (CFD) models are common and reliable tools for modeling HVAC applications. They were adopted in many modern studies including [5, 6]. Generally, CFD models should be powerful enough to describe several coexisting nonlinear flow phenomena [7]. These HVAC related phenomena include unsteadiness, turbulence, and buoyancy effects. Also, considerable effort should be allocated for grid generation. This is mainly due to the presence of complex boundaries [8]. Often numerous grid points are required to achieve adequate resolution. As a result, large linear systems need to be solved using special iterative methods. The rather popular commercial package ANSYS [9] is widely adopted [10-12]. This rather costly option is based on the

* *Corresponding author.*
E-mail address: Ahmed_7afez@outlook.com

https://doi.org/10.37934/arfmts.87.1.7690

finite volume method (FVM). On the other hand, works based on the finite element method (FEM) are very rare.

A major goal of the current study is clarifying the feasibility of modeling HVAC problems by FEM. Open-source packages are adopted for grid generation Salome Meca [13] and FEM (ELMER) [14]. This collection of packages is employed to deal with the complexities discussed. Simulation results are validated via comparison with full scale measurements [15]. The three-dimensional experimental setup is carefully discretized and detailed flow features are clarified. The model convergence, accuracy, and efficiency are illustrated.

2. Theoretical Model

3D model had been adopted using the k-ϵ Model. Reynolds-Averaged Navier-Stokes (RANS) to obtain a closed system of equations to model mean flow and fluctuating motion

- Incompressible flow: since compressibility effects can be neglected at the relatively low HVAC speeds.
- Modeling buoyancy forces adopting Boussinesq assumption: This is crucial to relate density and temperature variations within incompressible flow [16]
- Turbulent flow: Generally, HVAC flow is convection dominated. Mean flow is obtained using Reynolds-Averaged Navier-Stokes (RANS) k-ϵ Model.
- Unsteady flow: to capture transient or periodic phenomena
- Negligible viscous heating: due to low Reynolds number flow inside the ventilation room [17].
- Neglected air leakage: assuming very small sized room gaps [15]

As mentioned above for assumptions used in the CFD model to simplify mathematical model [18].
Conservation of Mass (Continuity Equation)

$$\nabla . \vec{u} = 0 \tag{1}$$

Conservation of Momentum (N.S)

$$\rho\left(\frac{\partial \vec{u}}{\partial t} + \vec{u} \,.\, \nabla\vec{u}\right) = -\nabla p + \nabla \,.\, \left((\mu + \mu_t)(\nabla\vec{u} + (\nabla\vec{u})^T)\right) + \rho g\big(1 - \beta(T - T_o)\big) \tag{2}$$

Conservation of Energy

$$\rho\left(\frac{\partial T}{\partial t} + (\vec{u} \,.\, \nabla)T\right) = \nabla \,.\, \left(\left(\frac{k_{th}}{c_p} + \frac{\mu_t}{\sigma_t}\right)\nabla T\right) \tag{3}$$

Turbulence Model (Standard $\mathrm{k} - \epsilon$))

- Turbulence Kinetic Energy (k)

$$\rho\left(\frac{\partial k}{\partial t} + \nabla \,.\, (\vec{u}k)\right) = \nabla . \left[\left(\mu + \frac{\mu_t}{\sigma_k}\right)\nabla k\right] + P_k + G_b - \rho\epsilon \tag{4}$$

- *Dissipation Rate of Turbulence Energy (ϵ).*

$$\rho\left(\frac{\partial \epsilon}{\partial t}+\nabla .(\vec{u}\epsilon)\right)=\nabla.\left[\left(\mu+\frac{\mu_t}{\sigma_\epsilon}\right)\nabla\epsilon\right]+C_{1\epsilon}\frac{\epsilon}{k}\left(P_k+G_b\right)-C_{2\epsilon}\rho\frac{\epsilon^2}{k} \quad (5)$$

where

- $\mu_t = C_\mu \frac{\rho k^2}{\epsilon}$ (Turbulent Viscosity).
- T_o, (Reference temperature = 25 °C)
- $\beta = \frac{1}{T_o}$ (Thermal expansion coefficient)
- k_{th} (Thermal conductivity of air)
- P_k (Production due to mean velocity shear).
- G_b (Production due to buoyancy).
- Constant Coefficients [19]
  $\sigma_k = 1.0, \sigma_\epsilon = 1.3, C_{1\epsilon} = 1.44, C_{2\epsilon} = 1.92, C_\mu = 0.09$

Initial conditions values of the whole room domain for velocity field are zero in the all directions u, v, w = 0, for temperature is $27\ ^\circ C$ and for turbulence variables $k = 6.121e-6\ m^2/s^2$, $\epsilon = 2.308e-8\ m^2/S^3$ which calculated from [9] by:

$$k = \frac{3}{2}\left(u_{avg} * I\right)^2 \quad (7)$$

$$\epsilon = C_\mu^{3/4}\frac{K^{3/2}}{l} \quad (8)$$

where

- u_{avg} is the mean flow velocity.
- I *is turbulence intensity* $\approx 1\% - 5\%$
- C_μ *is empirical constant* $= 0.09$
- l *is length scale* $= 0.07 * Charaterstic\ Length$

Boundary conditions for the model room consist of four different conditions as shown in Figure 1

- Wall:No-slip condition and Adiabatic.
- Heat Sources: No-slip condition and generated power ($600\ W$).
- Inlet: Flow rate ($300\ m^3/h$), temperature 15.3 $^\circ C$ and estimated turbulence variables from Eq. (7) and (8) $k = 6.121e-6\ m^2/s^2$ & $\epsilon = 2.308e-8\ m^2/s^3$
- Outlet: Exit pressure is atmospheric pressure.

3. Full Scale Measurement Setup

The experiments were conducted in set-up in a full-scale room in Aalborg University [15] with the geometry shown in Figure 1.

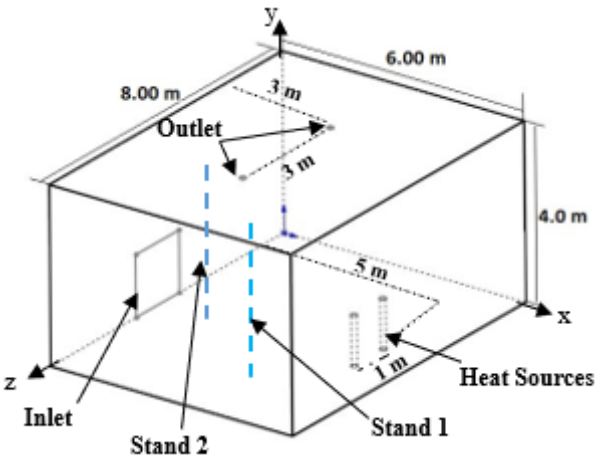

Fig. 1. Aalborg University Room Domain Geometry

Geometry configuration description of the room is the length = 6.0 m (x-direction), the width = 8.0 m (z-direction) and the height = 4.0 m (y-direction). Cooled airflow enters from the inlet diffuser in the center bottom of left wall with dimensions (1.375 m×1.5 m) then exit from two outlet slots in the ceiling with a diameter (0.15 m) after mixing with hot buoyancy driven flow because of power generation from two cylinders heat sources with dimensions (0.15 m×1.125 m).

The measurements had been taken along the vertical stands, stand 1 at (x = 4.0 m, z = 7.0 m) to measure temperature distribution at a location of the room where no direct effect of heat sources and inlet diffuser also stand 2 at (x = 2 m, z = 4.0 m) to measure velocity profile at symmetry plane of room.

4. Numerical Model

4.1 Space Discretization

CFD simulation was done using Open-Source code, finite element method (FEM) package ELMER. A brief review is provided for the FEM method for a concise presentation. The interested reader is referred to any standard textbook [20]. Unlike finite difference methods, FEM possesses the advantage of handling complex geometries while avoiding complicated grid transformations. Once the domain is discretized using suitable structured or unstructured mesh, variables are interpolated over each element. A suitable integral weak form is adopted for numerical discretization. Boundary conditions are enforced using contour integrals. Domain integrals done over each separate element are added together and global algebraic systems are obtained. A widespread integral formulation is the method of weighted residuals (MWR), adopting Galerkin method approximation. This can be described as [21]

$$\int_v R(x,y,z) \times W(x,y,z)\, dv = 0 \tag{6}$$

Here, R(x,y,z) is the residual equated to the governing equations set differential equation, Eq. (1)-(5). W(x,y,z) is the weight function equated to the interpolation basis function according to Galerkin approximation.

4.2 Time Discretization and Nonlinear Systems

A rather powerful feature of ELMER is adaptive implicit first order time stepping [22]. A trial time step $\Delta t = \Delta t_r$ is adopted. Next, the solution is recomputed using two time steps of size $\Delta t_r/2$. Both solutions are compared, and Δt_r is accepted if the difference is small enough. Among many numerical parameters specified by the user, the minimum time step $(\Delta t)_{min}$ is of special importance. This is the minimum allowed time step value.

The nonlinear nature of the flow equations is treated in ELMER within a rigor framework [23]. This is clarified in Figure 2. The outermost loop is the time stepping algorithm already discussed. Internal steady state iterations (maximum number $N_{s.s}$) within each time step re performed. Within each of these, nonlinear Picard iterations (maximum number N_{nl}) are needed to connect various components $(N.S\,, k-\epsilon\,, Energy)$. Finally, the inner most loop is needed to solve linear systems. The iterative BiCGStabl method (maximum number N_l) is used with ILU1 Preconditioning. In addition to the maximum number of loops per iteration, convergence tolerances should be specified.

Selection of extremely high or low values for maximum iterations per loop leads to very slow or numerically unstable computations, respectively. Convergence tolerances are subject to similar considerations The values provided in Table 1 are based on numerical experiments and recommendations on ELMER guide [22].

Table 1
Iterations Number (Steady State, Non-linear, Linear)

Parameter	Value and definition
$N_{s.s}$	30 per each time step, Number of Iterations
N_{nl}	1 per each steady state iteration, Number of Iterations
N_l	2000 per each nonlinear iteration, Number of Iterations
$C_{s.s}$	10^{-5}, convergence tolerance for steady state iterations
C_{nl}	10^{-5}, convergence tolerance for nonlinear iterations
C_l	10^{-20}, convergence tolerance for linear iterations

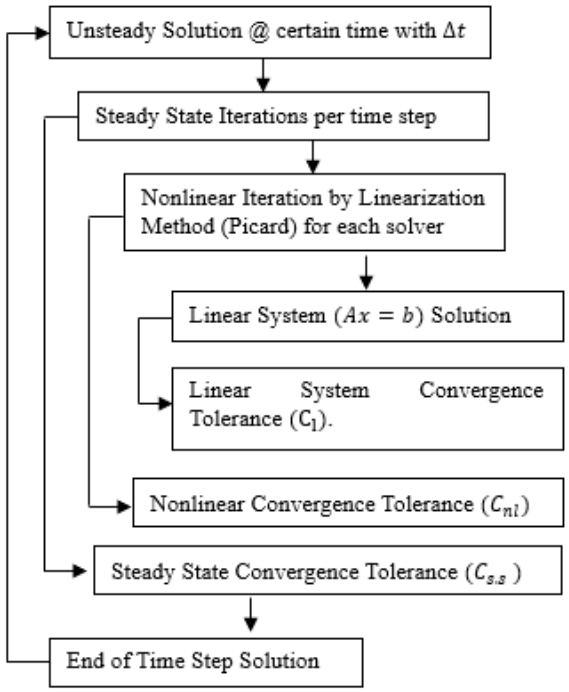

Fig. 2. Elmer Numerical Solution Technique

4.3 Parallel Computation

Parallel Computing is an essential requirement for three-dimensional simulations. This is another advantage in Elmer were parallel computation based on MPI library is provided [22]. Parallel computations rely on mesh decomposition to several sub-domains as shown in Figure 3. Usually, each sub-domain is assigned to a computational core, and calculations are performed in parallel. Next results of separate cores are merged after each iteration where suitable compatibility conditions are implemented.

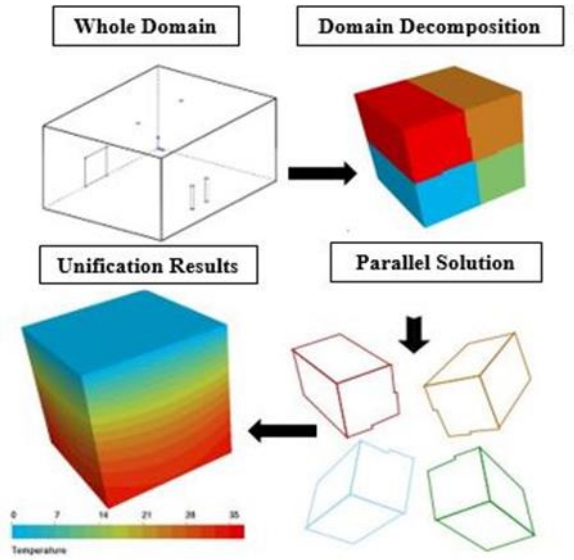

Fig. 3. Elmer Parallel Computing Technique

The server computer specs are 24 Cores processor, 24 gigabyte RAM. Typical computational time needed to reach a steady state was 480 hours.

4.4 Mesh Generation

Salome Meca Open-Source Software [13] is used for meshing. Unstructured meshes consisting of linear Tetrahedron elements are adopted. A sample cross-section is shown in Figure 4. Near walls, clustering can be well observed. Also, clustering is adopted near heat source boundaries. A typical tetrahedron linear element is shown in Figure 5. The main requirement of the turbulence model is achieving a small value of y^+. More details (definition and simulated values) are provided on the results section.

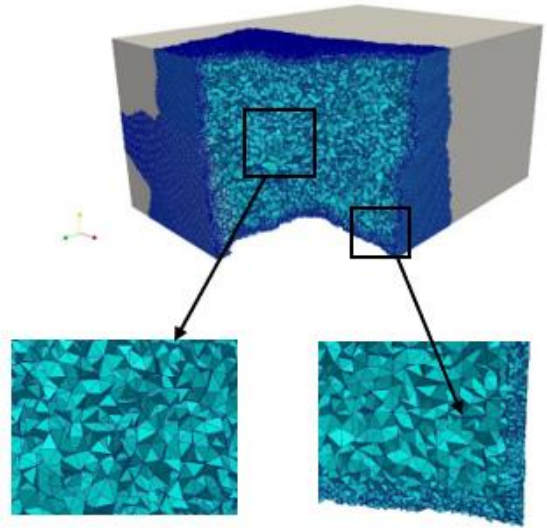

Fig. 4. Mesh Model 4.7 million Elements with Zoom to Show (Main Domain Elements, Clustering Wall Elements)

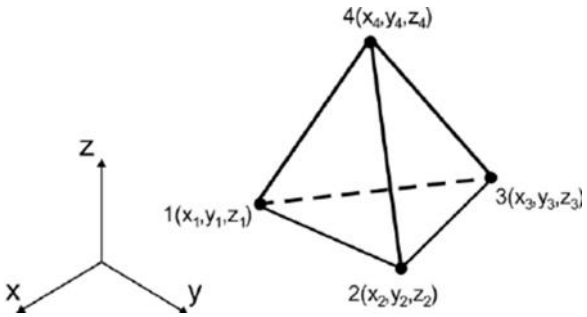

Fig. 5. Linear Tetrahedron Element Used in Meshing, defined in terms of 4 nodes

Three different mesh sizes were adopted, with a total number of 2.3, 3.5 and 4.7 million elements. This is necessary to clarify convergence. Typical values of mesh quality measures provided by Salome Meca software are shown in Table 2. These correspond to the finest mesh (4.7 million elements).

Table 2
Mesh Quality for 4.7 million Elements by Salome Meca

Quality Parameter	Value
Max (2D Aspect Ratio)	1.5
Max (3D Aspect Ratio)	2.5
Max (Skewness)	0.483

5. Results

ParaView Open-Source Software [24] was used for the post-processing step. Momentum and thermal field reached a steady state after 6 minutes of physical time. Various aspects of the results are discussed in the next subsection.

5.1 Model Validation

Among the three meshes, the finest mesh is used to display y^+contours at steady state. As shown in Figure 6 the range of y^+<5 is achieved. Consequently, turbulence model assumptions are fulfilled.

A ParaView calculator is used to calculate y^+ based on the following steps. Tangential velocity at wall nodes is obtained. Next, tangential velocity normal wall gradient $\left(\frac{\partial U}{\partial y}\right)_{@wall}$ is obtained. finally, the following relations are used [25]

$$\tau_w = \mu \left(\frac{\partial U}{\partial y}\right)_{@wall} \tag{9}$$

$$u_\tau = \sqrt{\frac{\tau_w}{\rho}} \tag{10}$$

$$y^+ = \frac{\rho y u_\tau}{\mu} \tag{11}$$

where

- τ_w is shear stress at walls.
- u_τ is friction velocity.
- y is the first layer thickness of mesh at walls.

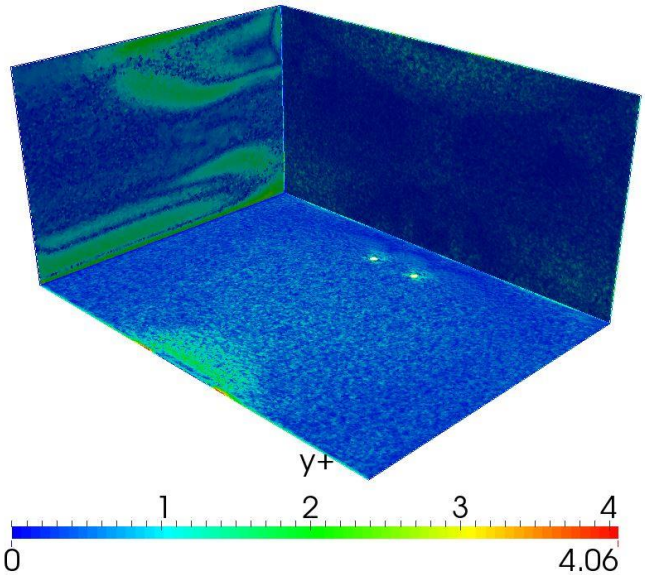

Fig. 6. y+ Range on Walls for Mesh Model (4.7 million elements)

CFD solutions for the three meshes models are displayed with experimental results at stand 1 (temperature), in Figure 7 and stand 2 (velocity) in Figure 8.

Non-dimensional values $\left(\frac{T(x)-T_{in}}{T_e-T_{in}}\right)$ are displayed along the vertical dimensionless y-axis (normalized w.r.t. room height $H = 4.0m$). Here T_{in} , T_e are inlet temperature and exit temperatures, respectively.

The results of the three meshes are almost identical. However, considering the velocity profile, the situation is different. The velocity magnitude is plotted versus the dimensionless height. The enhanced accuracy of grid refinement is well clarified.

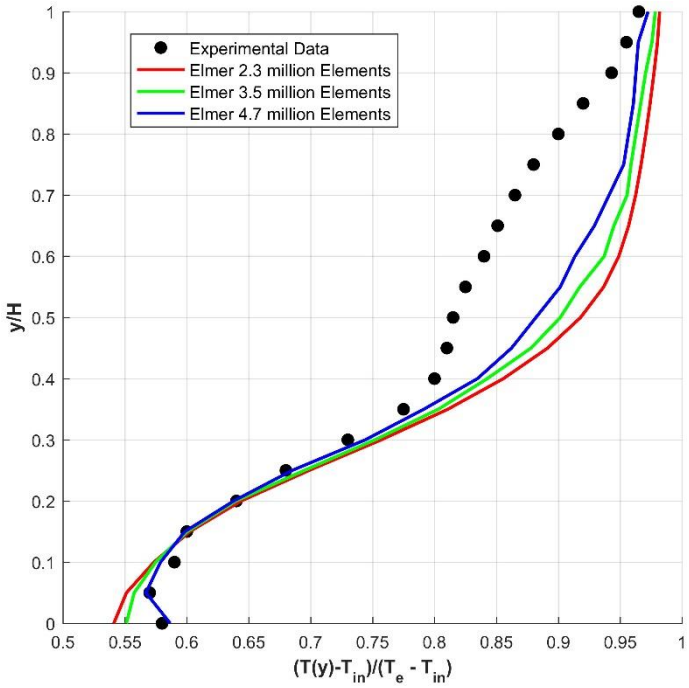

Fig. 7. Temperature Distribution Validation Along the y-axis

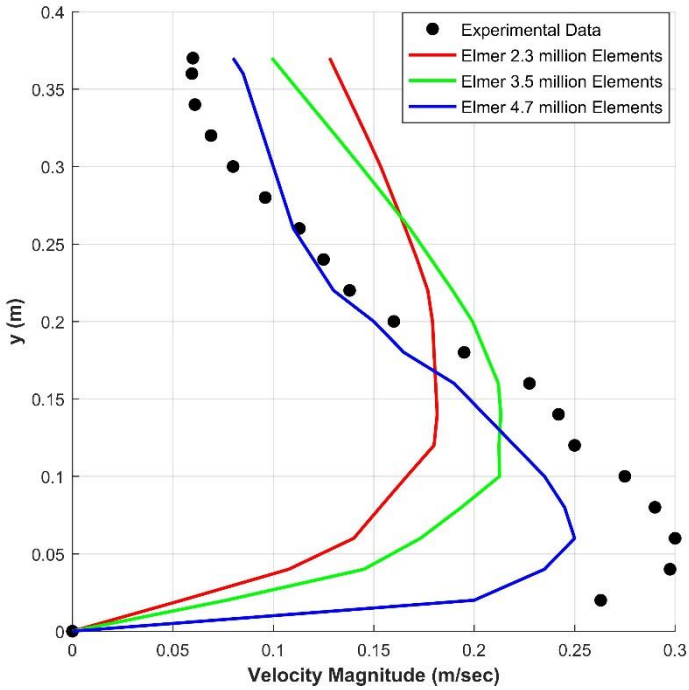

Fig. 8. Velocity Distribution Validation in Room Lower Part

5.2 Comparison with 2D Model

In order to clarify the relevance of three-dimensional modeling, a two-dimensional simplified setup is simulated. The problem is assumed to be symmetric at a middle vertical plane. The details are shown in Figure 9. The vertical dimensions for the two-dimensional case are identical to those of the full-scale measurements. Also, the same inlet flow rate and heat source power are adopted. An unstructured mesh (125,592 triangular elements) was generated by Salome Meca as shown in Figure 10. Two-dimensional simulated temperature contours are shown for two instants t = 10, 245 secs in Figure 11. The transient effect of the cold inlet can be well observed. Also, buoyancy effects produce a thermal plume above the heat source. However, the steady state results show an artificially shielded region behind the heat source. There is not any mechanism to generate this isolated region in the real three-dimensional setup.

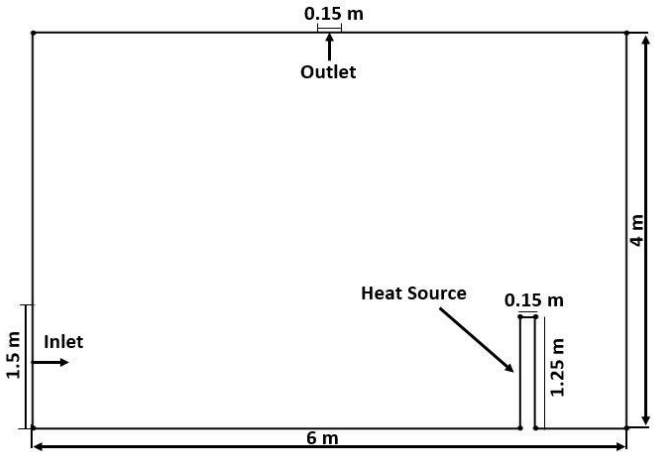

Fig. 9. 2D Aalborg university Model Geometry

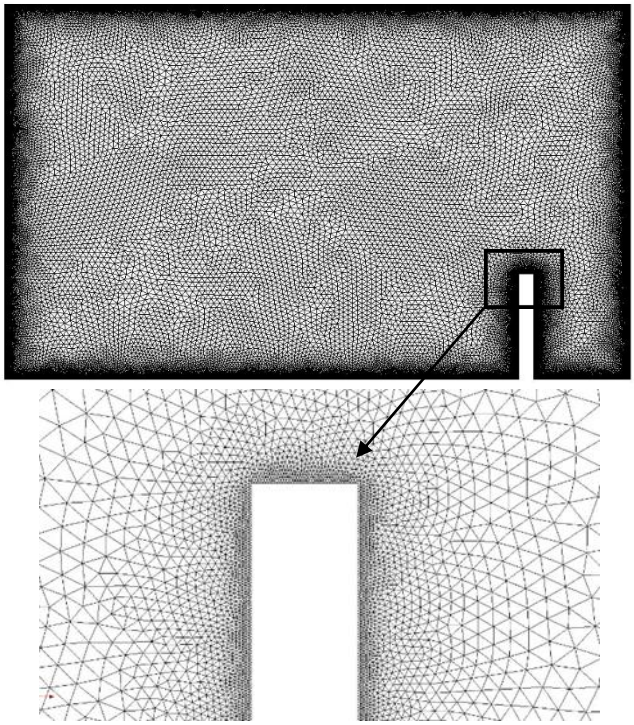

Fig.10. 2D Mesh Generation (125592) Elements

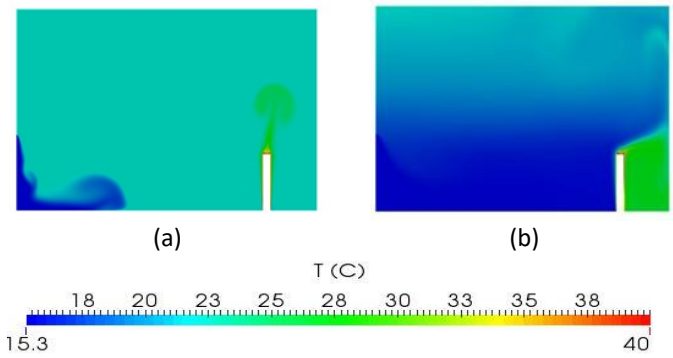

Fig. 11. 2D Temperature Contours (a) t = 10 sec, (b) t = 245 sec

5.3 3D Model Transient Results

Three-dimensional transient flow field is presented in Figure 12, 13 and 14 Snapshots are provided at four instants. To clarify the three-dimensional behavior, contours are projected and displayed at three orthogonal planes. As already mentioned, steady state was achieved at $t = 6$ minutes. Starting with temperature contours in Figure 12, the transient cold inlet plume approaching the heat source can be well observed. The same observation is noted for the thermal plumes above the heat sources. However, the cooling effect is almost radiated in a three-dimensional trend. This is well clarified at the base (lower) plane. As expected, the fictitious isolated region behind heat sources (displayed in two-dimensional results) is totally missing.

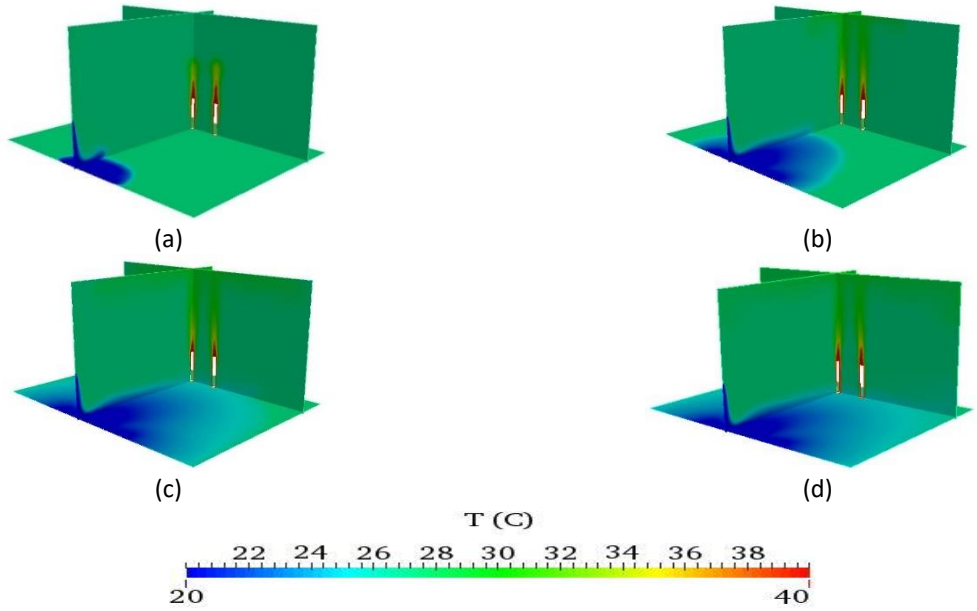

Fig. 12. 3D Temperature Distribution After Four Different Intervals: (a) After 10 sec (b) After 60 sec (c) After 180 sec (d) After 360 sec

Transient evolution of gauge pressure contours is displayed in Figure 13. The spatial variation is almost hydrostatic (variation only in the vertical direction). This is expected since the dynamics are mainly governed by temperature and buoyancy effects. However, the strong variation of pressure at the inlet and outlet (upper ceiling) can be well observed. In these two small regions, the pressure gradients influence is considerable.

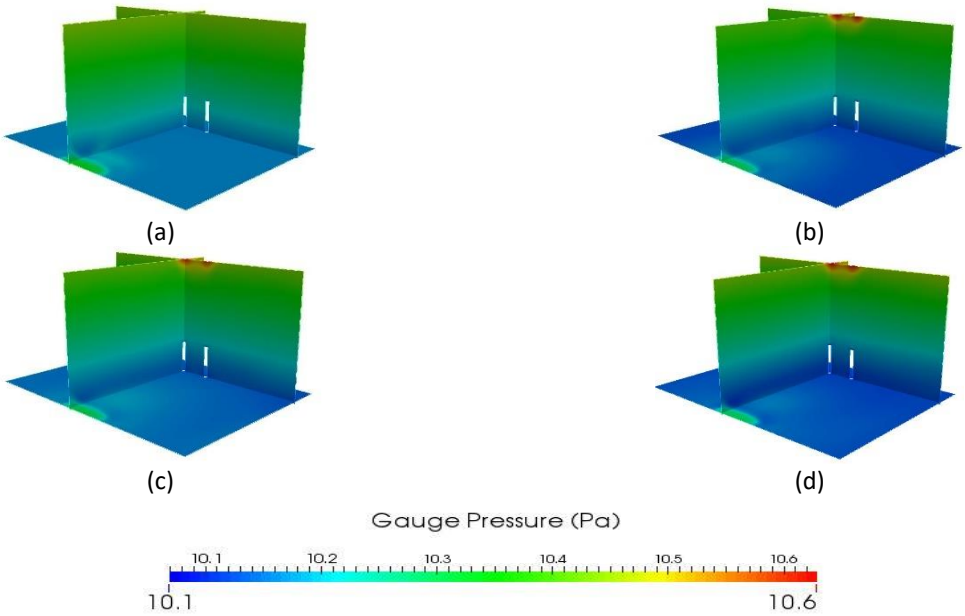

Fig. 13. 3D Gauge Pressure Distribution After Four Different Intervals: (a) After 10 sec., (b) After 60 sec., (c) After 180 sec, (d) After 360 sec

Spatial contours of turbulence parameter k are displayed in Figure 14 at the same four instants. High values of k are observed above heat sources and near the cold inlet. This is expected since the problem is mainly influenced by temperature gradients. Hence strong turbulence mixing is expected at regions of high temperature gradient.

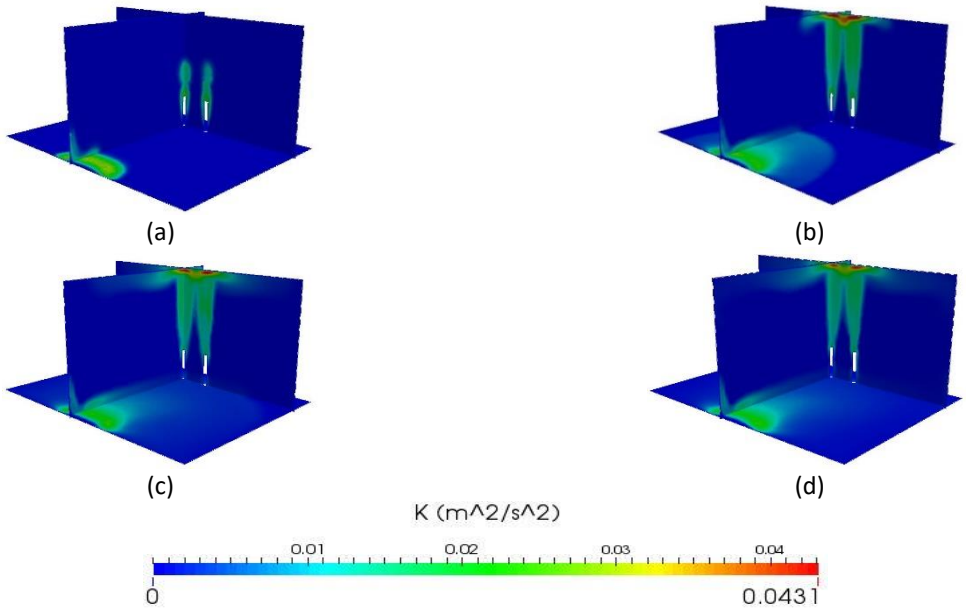

Fig. 14. 3D (TKE) Distribution After Four Different Intervals: (a) After 10 sec (b) After 60 sec (c) After 180 sec (d) After 360 sec

Finally, the complex velocity field is presented at steady state in Figure 15. In order to clarify the flow structure, zoomed plots are provided also in Figure 15. A strong vortex is generated at the upper left corner. This is attributed to the strong uprising hot air stream above the heat sources. The behavior at the vertical section somehow similar to the classical driven lid problem. The zoomed plot

neat the bottom of the heat sources clarifies the buoyancy effects, where air particles are sucked upwards.

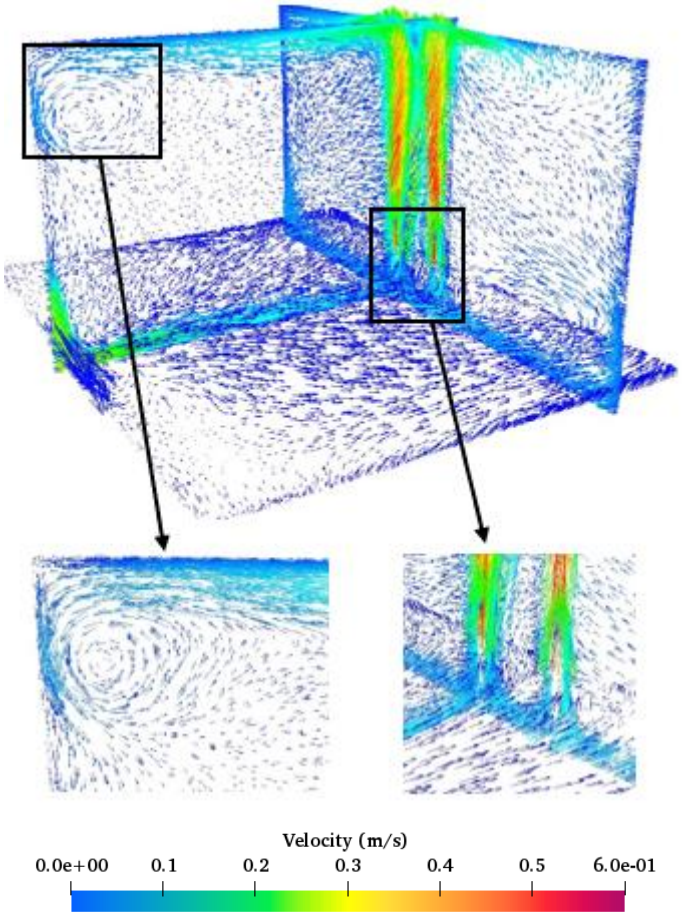

Fig. 15. Steady State 3D Velocity Vectors After 360 Sec

6. Conclusion

A three-dimensional model for HVAC applications is provided. The model is verified by comparison with full scale experimental measurements. Converged, three dimensional transient results are obtained adopting suitable mesh size (4.7 million elements) within available computational resources (480 server hours). Transient flow features are illustrated, including the cold inlet thermal plume. Adopting a three-dimensional model is crucial to avoid nonphysical predictions produced by two dimensional simulations. For instance, the problem of fictitious isolated regions behind cylindrical obstacles is eliminated. The flow behavior is well explained physically. The dominant effect of cold inlet and heat sources, is well captured as buoyancy driven plumes, accompanied by strong turbulence. Future works should focus on more realistic scenarios, including complex geometries and perforated inlets.

Acknowledgments
This research was supported by Aerospace Engineering Department at Cairo University. The authors would like to express their deep gratitude to Prof. Ahmed Rashed, for managing access to the computational.

References

[1] Pérez-Lombard, Luis, José Ortiz, and Christine Pout. "A review on buildings energy consumption information." *Energy and buildings* 40, no. 3 (2008): 394-398. https://doi.org/10.1016/j.enbuild.2007.03.007
[2] Lubis, Hamzah. "Renewable Energy of Rice Husk for Reducing Fossil Energy in Indonesia." *Journal of Advanced Research in Applied Sciences and Engineering Technology* 11, no. 1 (2018): 17-22.
[3] Davis, Lucas W., and Paul J. Gertler. "Contribution of air conditioning adoption to future energy use under global warming." *Proceedings of the National Academy of Sciences* 112, no. 19 (2015): 5962-5967. https://doi.org/10.1073/pnas.1423558112
[4] Coad, William J., Ronald Hunter Howell, and Harry J. Sauer Jr. "Principles of heating, ventilating, and air conditioning." (2005).
[5] Jian, Qifei, Qiaoli Wang, Haoting Wang, and Zheng Zuo. "Comparison between numerical and experimental results of airflow distribution in diffuser based data center." (2012): 011006. https://doi.org/10.1115/1.4005912
[6] Fulpagare, Yogesh, and Atul Bhargav. "Advances in data center thermal management." *Renewable and Sustainable Energy Reviews* 43 (2015): 981-996. https://doi.org/10.1016/j.rser.2014.11.056
[7] Muhammad, Nura Muaz, Nor Azwadi Che Sidik, Aminuddin Saat, Yusuf Alhassan, and Yutaka Asako. "A Numerical Investigation on the Combined Effect of Aluminum-Nitride/Water Nanofluid with Different Mini-Scale Geometries for Passive Hydrothermal Augmentation." *Journal of Advanced Research in Numerical Heat Transfer* 1, no. 1 (2020): 1-12.
[8] Fohimi, Nor Azirah Mohd, Muhammad Hanif Asror, Rosniza Rabilah, Mohd Mahadzir Mohammud, Mohd Fauzi Ismail, and Farid Nasir Ani. "CFD Simulation on Ventilation of an Indoor Atrium Space." *CFD Letters* 12, no. 5 (2020): 52-59. https://doi.org/10.37934/cfdl.12.5.5259
[9] Inc, A. N. S. Y. S. "ANSYS FLUENT theory guide." *ANSYS, Inc Canonsburg* (2013). https://doi.org/10.1016/0140-3664(87)90311-2
[10] Nada, S. A., and M. A. Said. "Effect of CRAC units layout on thermal management of data center." *Applied thermal engineering* 118 (2017): 339-344. https://doi.org/10.1016/j.applthermaleng.2017.03.003
[11] Hoang, Hong-Minh, Steven Duret, Denis Flick, and Onrawee Laguerre. "Preliminary study of airflow and heat transfer in a cold room filled with apple pallets: Comparison between two modelling approaches and experimental results." *Applied Thermal Engineering* 76 (2015): 367-381. https://doi.org/10.1016/j.applthermaleng.2014.11.012
[12] Ismail, Mohd Azmi, and Mohd Sabri Che Jamil. "CFD HVAC Study of Modular Badminton Hall." *CFD Letters* 12, no. 7 (2020): 90-99. https://doi.org/10.37934/cfdl.12.7.9099
[13] G. N. U. Fdl, "Salome-Meca User Guide Overview," 2016. [Online].Available: https://www.codeaster.org/UPLOAD/DOC/Formations/01-overview-2.pdf.
[14] P. Råback and M. Malinen, "Overview of Elmer," 2019. [Online].Available: http://www.nic.funet.fi/index/elmer/doc/ElmerOverview.pdf.
[15] Jacobsen, Torsten V., and Peter V. Nielsen. "Numerical modelling of thermal environment in a displacement-ventilated room." (1993).
[16] Demuren, Ayodeji, and Holger Grotjans. "Buoyancy-driven flows—Beyond the boussinesq approximation." *Numerical Heat Transfer, Part B: Fundamentals* 56, no. 1 (2009): 1-22. https://doi.org/10.1080/10407790902970080
[17] Dorfman, Abram S. *Applications of mathematical heat transfer and fluid flow models in engineering and medicine*. John Wiley & Sons, 2017. https://doi.org/10.1002/9781119320715
[18] Başkaya, Şenol, and Emre Eken. "Numerical investigation of air flow inside an office room under various ventilation conditions." *Pamukkale University Journal of Engineering Sciences* 12, no. 1 (2011).
[19] Launder, Brian Edward, and Bahrat I. Sharma. "Application of the energy-dissipation model of turbulence to the calculation of flow near a spinning disc." *Letters in heat and mass transfer* 1, no. 2 (1974): 131-137. https://doi.org/10.1016/0094-4548(74)90150-7
[20] Chung, T. J. *Computational fluid dynamics*. Cambridge university press, 2010.
[21] Lewis, Roland W., Perumal Nithiarasu, and Kankanhalli N. Seetharamu. *Fundamentals of the finite element method for heat and fluid flow*. John Wiley & Sons, 2004.
[22] J. Ruokolainen, M. Malinen, P. Raback, T. Zwinger, A. Pursula, and M. Byckling, "ElmerSolver Manual," Finland, 2019. [Online]. Available: http://www.csc.fi/elmer/documentation.
[23] Elmerteam, "ElmerSolver Input File (SIF) Explained," Finland, 2018. [Online]. Available:. http://www.csc.fi/elmer/documentation.
[24] Squillacote, Amy Henderson, James Ahrens, Charles Law, Berk Geveci, Kenneth Moreland, and Brad King. *The paraview guide*. Vol. 366. Clifton Park, NY: Kitware, 2007.

[25] Neale, A., Derome, D., Blocken, B. and Carmeliet, J., 2006. CFD calculation of convective heat transfer coefficients and validation–Part 2: Turbulent flow. *International Energy Agency-ECBCS Annex*, *41*.